Interactions Between Transition-Metal Surfaces and MoS_2 Monolayers: Implications for Hydrogen Evolution and CO_2 Reduction Reactions

Avdhoot Datar,[1] Maya Bar-Sadan,[2,3] and Ashwin Ramasubramaniam[1,*]

[1]Department of Mechanical and Industrial Engineering, University of Massachusetts, Amherst, MA 01003, U.S.A.

[2] Department of Chemistry, Ben-Gurion University of the Negev, Beer-Sheva 8410501, Israel

[3] Ilse Katz Institute for Nanoscale Science and Technology, Ben-Gurion University of the Negev, Beer-Sheva 8410501, Israel

Abstract

Transition-metal dichalcogenides (TMDs) such as molybdenum disulfide (MoS_2) are of significant current interest as inexpensive, earth-abundant catalysts for reactions such as electrochemical hydrogen evolution and CO_2 reduction. While several high-throughput studies have focused on understanding the relative activities of various TMDs, including their multiple phases, the role of support effects on modulating adsorbate–TMD interactions is less well studied. Here, focusing on MoS_2 as a model TMD, we employ density functional theory calculations to understand the interactions of monolayers of 2H, 1T, and 1T' phases of MoS_2 with three transition-metal (TM) supports—Au, Ag, and Cu. In particular, we study the interfacial energetics and charge-transfer interactions at monolayer MoS_2/TM interfaces, and correlate these with the energetic stabilization of the metastable 1T and T' phases. We also examine the role of Cu supports in modulating the interaction of the supported monolayers with adsorbates such as H and CO, whose adsorption free-energies can be considered as descriptors for hydrogen evolution and CO_2 reduction reactions. While pristine basal planes of MoS_2 are relatively unaffected by supports, vacancy-defects—well-known active sites in the MoS_2 basal plane—can be profoundly affected, to the extent that catalyst poisoning becomes a distinct possibility. Our studies demonstrate that support effects ought to be taken into consideration when screening 2D TMD catalysts, especially in the presence of strong charge-transfer interactions as might be expected at interfaces between electrodes and TMD catalysts.

Corresponding Author

*ashwin@engin.umass.edu

1. Introduction

Electrocatalytic energy conversion, integrated with renewable power sources, is a promising approach for sustainable energy conversion and storage. Catalysts play a vital role in these electrochemical processes, in particular, for reducing the overpotentials and improving the selectivity of products. In recent studies, transition-metal dichalcogenides (TMDs) have been widely investigated as electrocatalysts due to their low cost, stability, and catalytic activities that are comparable to noble-metals.[1–6] In the context of sustainable energy conversion, MoS_2—a well-known hydrodesulfurization catalyst[7,8]—has been studied extensively for the hydrogen evolution reaction (HER)[8,9] and the CO_2 reduction reaction (CO2RR).[10–12] MoS_2 was suggested as an appealing catalyst for water-splitting[13–15] and CO2RR[10] but it has yet to fulfil its promise in practical applications.

CO2RR is a promising electrocatalytic reaction, due to its potential to mitigate rising CO_2 levels in the atmosphere while generating hydrocarbons for a sustainable carbon-based economy. Theoretical work by Nørskov and coworkers has suggested that transition-metal (TM) doping can improve the CO2RR activity of MoS_2.[16] They have also shown that the linear scaling relationship in adsorption energy of intermediates – a bottleneck in CO2RR – can be broken on MoS_2 edges, by binding CO* to dopant metal site and by covalent binding of other intermediates at chalcogen sites.[16] Salehi-Khojin and coworkers have shown that Mo-terminated edges of MoS_2 efficiently convert CO_2 to CO in ionic liquids.[10–12] Francis et. al observed propanol formation with MoS_2 as electrocatalyst in CO2RR;[17] they also showed that increasing density of edges resulted in lower propanol formation, indicating that the basal plane of MoS_2 is active for propanol formation in CO2RR.[17] However, the performance of these electrocatalysts for CO2RR are hindered by sluggish kinetics, multiple products accompanied by poor selectivity, and a strong competition with HER. In the context of HER, several recent studies have shown that MoS_2 may contain excellent catalytic sites, which are competitive with Pt for electrocatalysis.[18–23] The major catalytic activity of MoS_2 is observed from the edge sites while basal planes are inert towards HER. Hence, various studies have focused on increasing the density of edge sites for boosting catalytic activity.[24–26] Yet, the overall performance of MoS_2 based catalyst remains limited due to the relatively small fraction of active sites and lower electrical conductivity of semiconducting 2H phase of MoS_2. Thus, synthesizing stable MoS_2 based catalysts with a high number of active sites and improved electrical conductivity remains an ongoing challenge, especially for commercially-viable catalysts.

The semimetallic 1T and 1T′ phases of MoS_2 have attracted interest and shows superior catalytic activity for HER relative to the stable 2H phase.[27–29] However, the main problem in employing the 1T or 1T′ phases of MoS_2 for catalysis is that these phases are metastable and easily converted to the less active

but more stable 2H phase.[30] Studies have shown that the metastable, metallic phases can be stabilized with respect to the 2H phase by intercalating alkali metals in van der Waals gap of MoS_2,[31] adsorbing transition metal adatoms,[32] or by creating chalcogen vacancy defects.[33,34] Computational and experimental studies have pointed out that electron transfer is a key factor in stabilizing 1T/1T′ phases of TMDs over 2H phase.[32,35,36] In recent work, Au@MoS_2 core-shell nanoparticles were shown to act as better catalysts for HER than freestanding MoS_2 (nanoflowers) and the origin of this enhanced activity was shown to arise due to electron transfer from the metallic Au core to the semiconducting 2H MoS_2 shell.[37] Furthermore, a phase transition to 1T MoS_2 was also reported for core-shell nanoparticles with semiconducting $Cu_{2-x}S$ as core and MoS_2 as shell; the 1T phase was shown to form preferentially at Cu-terminated faces of $Cu_{2-x}S$ whereas the S-terminated faces were covered in 2H MoS_2 shells.[38] A recent study of Ag@MoS_2 core-shell nanoparticles has also shown that these hybrid structures display superior electrocatalytic activity over MoS_2 nanosheets.[39] Thus, it is intriguing to investigate how electron transfer from metallic supports (or cores) can in general modulate the catalytic properties of supported MoS_2 monolayers and possibly even stabilize the metastable 1T/1T′ phases over the 2H phase via a charge-transfer induced phase transition.

In this paper, we study and contrast the effect of Cu, Ag, and Au supports on the phase stability and catalytic activity of monolayer MoS_2. Figure 1 displays the work functions of (111) and (100) surfaces of these transition metals (TM) elements relative to the work functions of the 1T/1T′ phases and the band edges of the 2H phase. Based on these level alignments, the three chosen transition metals are expected to display charge-transfer interactions of varying strengths with the 1T and 1T′ phases, with very little charge transfer in the case of Au and maximum charge transfer in the case of Ag. The interaction between the transition metals and 2H MoS_2 are expected to be generally weaker than with the 1T/1T′ phases but here, again, the hierarchy of interactions is expected to range from weakest for Au to strongest for Ag. Thus, with these three candidate transition-metal supports it is possible to systematically evaluate the influence of charge-transfer interactions on electron doping and potential phase transitions in supported MoS_2 monolayers, as well as the implications for molecular adsorption on the supported MoS_2 phases.

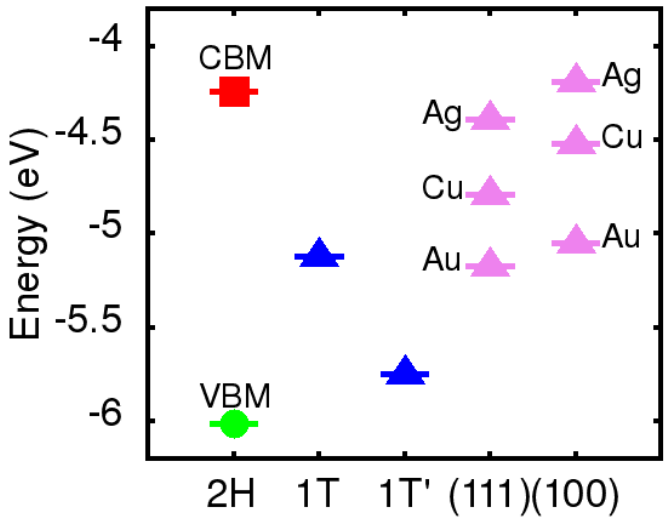

Figure 1: Work functions of (111) and (100) surfaces of Au, Ag, and Cu, and monolayers of 1T and 1T′ phases of MoS_2; the valence band maximum (VBM) and conduction band minimum (CBM) energies of monolayer 2H MoS_2 are also indicated; all energies are relative to the vacuum level (zero).

The remainder of this paper is organized as follows. In Section 2, we present details of the computational methods and simulation models. In Section 3, we discuss our findings on the thermodynamic stability and electronic structure of MoS_2 phases on Au, Ag, and Cu supports, as well the energetics of H and CO adsorption on these phases with Cu supports. Concluding remarks are provided in Section 4.

2. Computational Methods

Density functional theory (DFT) calculations were performed using the Vienna Ab Initio Simulation Package (VASP).[40,41] The core and valence electrons were described using the projector-augmented wave (PAW) method [42,43] and the Perdew-Burke-Ernzerhof (PBE) form [44] of the generalized-gradient approximation was used to describe electron exchange and correlation. The kinetic energy cutoff was set to 400 eV and a Gaussian smearing of 0.05 eV was used for Brillouin-zone integrations. Atomic positions were optimized using the conjugate-gradient method with a force tolerance of 0.01 eV/Å. The relaxed lattice parameters for single-layer 2H and 1T MoS2 phases were found to be 3.19 Å, and 3.16 Å, respectively; for the 1T′ phase the unit cell dimensions were found to be 5.72 Å × 3.17 Å. The calculated lattice parameters are in good agreement with previous studies.[45,46] Bulk lattice parameters for transition

metals (TM) Au, Ag, and Cu were calculated to be 4.16 Å, 4.16 Å, and 3.63 Å, respectively, and are also in good agreement with prior reports.[47]

Models of MoS_2 monolayers of various phases supported on transition-metal (TM) slabs (Figure 2) were generated using the CellMatch program;[48] as MoS_2 and the TM supports are not lattice matched, the supercells were chosen to minimize the mismatch strain in the MoS_2 layer while keeping the number of atoms in the supercell tractable. The TM supports were modeled as slabs consisting of four layers in which atoms of the two bottommost layers were frozen at their bulk atomic positions. The upper two layers of the TM slab and the adsorbed MoS_2 layer were fully relaxed in all calculations. To avoid spurious interactions between periodic images, at least 15 Å of vacuum was inserted normal to the slabs. Atomic positions and cell vectors of the optimized MoS_2/TM supercells are provided in the Table S2. Typical distances between TM slabs and the bottommost layer of S atoms in MoS_2 are between 2-3 Å. Dipole corrections were applied in all calculations along the direction normal to the slabs.[49,50] The Brillouin zones of all MoS_2/TM supercells were sampled using a 5×5×1 Γ-centered *k*-point mesh. Bader analyses [51–53] were performed to calculate charge transfer between the TM-supports and the MoS_2

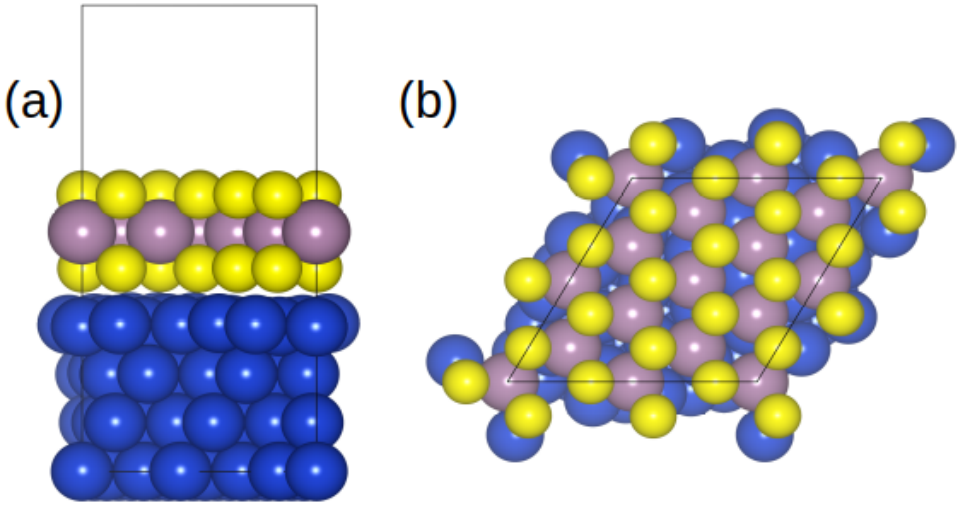

Figure 2: (a) Side and (b) top views of a representative slab model displaying monolayer 2H-MoS_2 on a Cu support. Blue, yellow, and grey spheres represent Cu, S, and Mo atoms, respectively.

monolayers.

All calculations of H and CO adsorption on isolated (unsupported) defect-free and defective monolayer MoS_2 phases were performed using 4×4 supercells. For studying the adsorption of H and CO on freestanding and TM-supported MoS_2, dispersion interactions were taken into account by applying

Grimme's PBE-D3 corrections.[54] As a first approximation, similar to prior studies,[16,55–57] we have neglected solvent effects and the overall conclusions are not expected to be altered qualitatively.

Vibrational entropies, S_{vib}, which are required for estimating adsorption free-energies of H and CO, are calculated by displacing the adsorbate atoms from their equilibrium positions by ± 0.015 Å in all three Cartesian directions, and diagonalizing the mass-weighted Hessian matrix to obtain the vibrational frequencies ω_i. The vibrational entropy, S_{vib}, may then be estimated as,[58]

$$S_{vib} = k_B \sum_{i=1}^{N} \left[-\ln\left(1 - e^{-\frac{\hbar\omega_i}{k_B T}}\right) + \frac{\hbar\omega_i / k_B T}{e^{\frac{\hbar\omega_i}{k_B T}} - 1} \right] \quad (1)$$

where k_B is Boltzmann's constant, T is the temperature (here, T=300K), ω_i is the vibrational frequency and N is the total number of vibrational modes. For gas-phase H_2 and CO molecules, we used standard entropies from the NIST database.[59] The vibrational frequencies were also used to calculate the zero-point energies of adsorbed and gas-phase species, defined as $E_{ZPE} = \sum_i \hbar\omega_i/2$. Differences between adsorbed and gas-phase entropies and zero-point energies can then be used to calculate the ΔS and ΔE_{ZPE} terms required for estimating the Gibbs free-energies of adsorption (*vide infra*).

3. Results and discussion

3.1 Effect of TM Supports on MoS_2 Phase Stability and Electronic Structure

A monolayer of MoS_2 is comprised of a layer of Mo atoms sandwiched between layers of S atoms. 2H MoS_2 has a trigonal prismatic structure (space group $P\bar{6}m2$) and the crystal field of the S atoms splits the 4*d* orbitals of Mo into three sets—in order of increasing energy—a_1 (d_z^2), e' (d_{xy}, $d_{x^2-y^2}$), and e'' (d_{yz}, d_{xz}).[60] The d_z^2-orbital is doubly occupied while the remaining *d* orbitals are unoccupied. Thus, electron transfer to 2H MoS_2 is energetically unfavourable, requiring the occupation of higher energy levels. On the other hand, the octahedral crystal field in 1T MoS_2 (space group $P\bar{3}m1$) splits the *d* orbitals into a lower energy t_{2g} set (d_{xy}, d_{yz}, and d_{xz}) and a higher energy e_g set (d_z^2 and $d_{x^2-y^2}$).[60] The t_{2g} orbitals are only partially occupied and can accommodate another electron upon addition of charge. Thus, there is a thermodynamic driving force for a 2H-to-1T phase transition with electron doping as reported both experimentally and theoretically.[31,32,61] It is also well known that the 1T phase can undergo a Peierls distortion to form a 1T′ phase of lower symmetry (space group $P2_1/m$);[62,63] the splitting of Mo *d* orbitals in 1T′ MoS_2 is similar to that in 1T-MoS_2.[64] Freestanding (isolated) monolayers of MoS_2 are most stable in the semiconducting 2H form, while metallic 1T and 1T′ forms are less stable, per MoS_2 formula unit (f.u.), by 0.83 eV/f.u. and 0.54 eV/f.u., respectively.[46] Support interactions can potentially affect the

phase stability of MoS_2 monolayers, while also modifying their electronic structure and catalytic activity; we consider these effects with Au, Ag, and Cu supports next.

For each combination of MoS_2 phase (2H, 1T, and 1T′) and TM support (Au, Ag, and Cu), we generated slab models with (111) and (100) surfaces facets for the support; these are the lowest energy surfaces for fcc metals. Furthermore to rule out, at least qualitatively, spurious effects from mismatch strains, we considered two levels of strain (Model 1 and Model 2; see Table S1 and Figure S1) for the MoS_2/TM(111) cases. Here, we report only on the results for Model 1 with the results for Model 2, being qualitatively similar, relegated to the SI. Given the computational cost of these large slab models, and informed by the results of the MoS_2/TM(111) cases wherein trends in interfacial energetics are consistent between the two sets of models, we only consider one set of models for the MoS_2/TM(100) cases. We

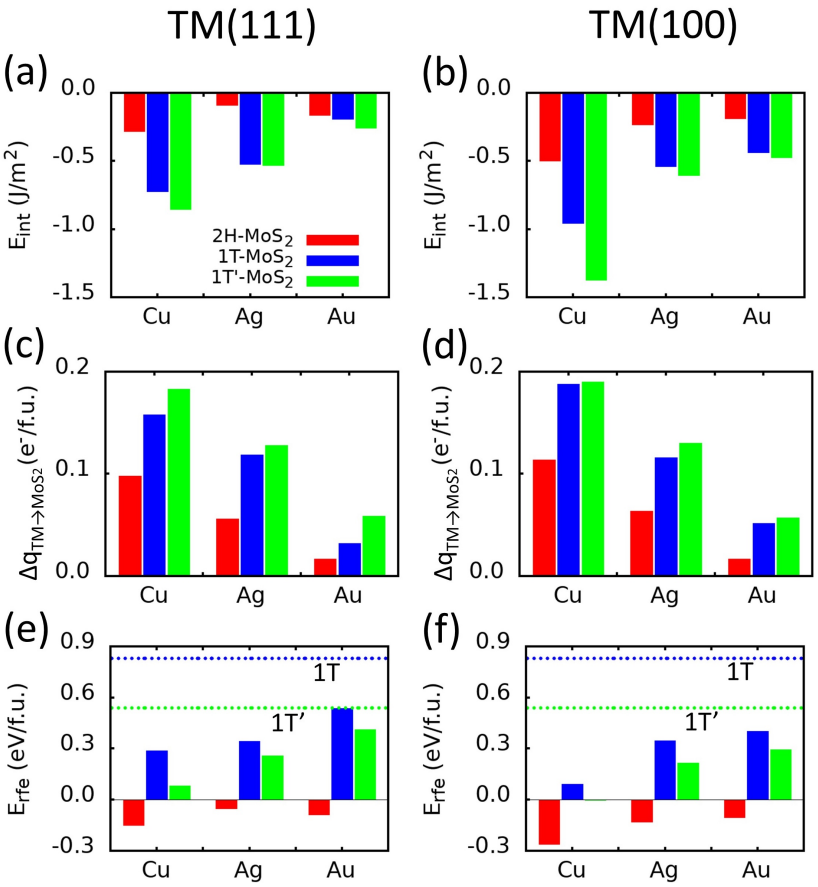

Figure 3: (a, b) Interface energies, E_{int}, per unit area for monolayer MoS_2/TM(111) and MoS_2/TM(100) interfaces. (c, d) Charge (in electrons, e^-) transferred from TM slab to monolayer MoS_2 per formula unit (f.u.), $\Delta q_{TM\rightarrow MoS_2}$, at MoS_2/TM(111) and MoS_2/TM(100) interfaces. (e, f) Formation energies relative to a freestanding 2H-MoS_2 monolayer, E_{rfe}, for MoS_2 phases supported on TM(111) and TM(100) surfaces; blue and green dotted lines represent E_{rfe} for freestanding 1T and 1T′ monolayers of MoS_2.

assess the stability of MoS_2/TM interfaces by calculating the interface energy per unit area, E_{int}, defined as

$$E_{int} = \frac{1}{A_{slab}}\left[E_{MoS_2/TM} - E_{TM} - E_{MoS_2}\right], \quad (1)$$

where $E_{MoS_2/TM}$ is the total (DFT) energy of the MoS_2/TM composite slab, E_{TM} is the energy of the TM slab alone, E_{MoS_2} is the energy of the isolated MoS_2 monolayer, and A_{slab} is the surface area of the slab. As defined, negative values of E_{int} correspond to the formation of stable interfaces. E_{int} is independent of the number of atoms in the system and/or the interface area, thus allowing for a direct comparison between the various supercells.

Figure 3(a) and Figure 3 (b) display the energies of the interfaces (E_{int}) that are formed upon supporting the three different phases of MoS_2 on TM(111) and TM(100) surfaces. In all cases, the interfaces energies are negative, indicating the formation of stable interfaces between MoS_2 and TM supports. In particular, a few key trends are evident from these data. First, the interface energies for a particular set of facets—(111) or (100)— and particular phase of MoS_2 increase in the order $E_{int}^{Au} < E_{int}^{Ag} < E_{int}^{Cu}$. This increased energetic stabilization in, going from Au to Ag to Cu, can be understood by noting that the surface energies, γ, of either the (111) or (100) set of facets are ordered as $\gamma^{Au} \approx \gamma^{Ag} < \gamma^{Cu}$; thus, at the simplest level of analysis, the formation of a more stable interface may be interpreted as the outcome of passivating a higher energy TM facet with a layer of MoS_2. The stronger interaction between the MoS_2 layers and higher energy facets is also reflected in the higher degree of charge transfer from the support to MoS_2, as calculated from a Bader analysis and reported in Fig. 3 (c) and Fig. 3(d). Second, for a particular phase of MoS_2, the interface formation energy is more negative for MoS_2/TM(100) interfaces than for MoS_2/TM(111) interfaces. This observation can again be explained by the fact that (100) facets of Au, Ag, and Cu, have higher surface energies than their (111) counterparts and thus, passivation by a MoS_2 layer has a stronger stabilizing effect on the (100) facets. The stronger interaction between MoS_2 and TM(100) facets, relative to TM(111) facets, is also reflected in the greater charge transfer between the support and MoS_2 in the former case [Fig. 3(c) and Fig. 3(d)]. Third, for every case of TM support and facet, the 2H-MoS_2/TM interfaces are the least stable followed by 1T-MoS_2/TM and 1T′-MoS_2/TM interfaces. This result is readily explained by the fact that the 2H phase is semiconducting, with no electronic states at the Fermi level that can interact strongly with supports, leading to a relatively inert basal plane. Specifically, from Figure 4, we see that the electronic density of states (DOS) of 2H-MoS_2 is only weakly perturbed upon adsorption on to a TM surface, supporting a picture of a charge-transfer dominated interaction rather than chemisorption. On the other hand, the 1T and 1T′ phases are metallic, with non-zero density of states at the Fermi level, and can thus interact more

strongly with the TM supports. This stronger interaction is clearly seen in the DOS plots of Figure 4 wherein we see both qualitative and quantitative changes in the DOS of the 1T and 1T′ MoS_2 monolayers upon adsorption on TM supports. In all cases studied here, we find that the interfacial stabilization is highest (more negative E_{int}) for 1T′-MoS_2/TM interfaces. Stronger interaction between metallic MoS_2 with TM supports is also reflected in shorter distances between MoS_2 and TM surfaces, for 1T and 1T′ phases with respect to 2H phase. Interestingly, we also observed that 1T phase undergoes a structural transformation to the 1T′ phase on interaction with TM supports.

The interface energy provides one metric of stability, assessing the thermodynamic feasibility of formation of the MoS_2/TM interface starting from the two separated constituents. However, we would also like to understand the thermodynamic phase preference of MoS_2 in the presence of a support: in other words, can relative ordering of unsupported phases be altered via strong interactions with a support? To this end, we quantify the relative stabilities of the supported phases of MoS_2 by calculating the relative formation energy per formula unit, E_{rfe}, defined as

$$E_{rfe} = \frac{1}{n_{MoS_2}}\left[E_{MoS_2/TM} - E_{TM} - n_{MoS_2}E_{2H-MoS_2}\right], \quad (2)$$

where n_{MoS_2} is the number of MoS_2 formula units in the supercell and E_{2H-MoS_2} is the energy of a single formula unit of a freestanding 2H-MoS_2 monolayer (at 0% strain), which is the ground state of an isolated monolayer. Figure 3(e) and Figure 3(f) display E_{rfe} for the various phases on MoS_2 adsorbed on TM(111) and TM(100) surfaces; the same data are reported in and Table 1 as the relative formation energy referenced to the 2H phase, ΔE_{rfe}. In all cases, we find that the 2H phase remains the thermodynamic ground state; even though the 1T and 1T′ phases undergo significant stabilization in the presence of supports, these phases are still metastable. Here again, we find that Cu—the support that interacts most strongly with MoS_2—exerts the greatest stabilizing effect on all phases. Interestingly, the 1T′ phase

Table 1: Relative formation energy referenced to the 2H phase, ΔE_{rfe}, per formula unit (eV/f.u.) of 1T and 1T′ MoS_2. ΔE_{rfe} for freestanding MoS_2 is calculated as, $\Delta E_{rfe} = E$ (1T/1T′ MoS_2) – E (2H MoS_2); for MoS_2/TM slabs this is calculated as $\Delta E_{rfe} = E_{rfe}$ (1T/1T′ MoS_2/TM) – E_{rfe} (2H MoS_2/TM).

ΔE_{rfe} (eV/f.u.)	Freestanding	MoS_2/Cu		MoS_2/Au		MoS_2/Ag	
		(111)	(100)	(111)	(100)	(111)	(100)
1T	0.83	0.43	0.36	0.63	0.51	0.39	0.48
1T′	0.54	0.23	0.26	0.50	0.40	0.31	0.35

becomes nearly thermodynamically stable on Cu(111) and Cu(100) surfaces, suggesting that this metastable phase might be easier to realize on supports than in freestanding nanostructures (e.g., nanoflowers); moreover, the energy difference between the supported 1T′ and 2H phases is now smaller (~0.3 eV/f.u.) than in the unsupported state (0.58 eV/f.u.), which should reduce the driving force for the undesirable 1T′-to-2H phase transition. Nevertheless, we reiterate that the extent of charge transfer in all of these cases is insufficient to induce a semiconductor-to-metal transition; while one could conceivably employ metals supports with higher work functions, these supports will likely be sufficiently reactive that the interfaces are already oxidized and/or sulfidized[38] prior to adsorption of MoS_2.

In summary, our thermodynamic and electronic structure calculations indicate that, of the various TM supports (Au, Ag, Cu) studied here, Cu is the most promising candidate for electron doping of MoS_2. Au is essentially inert and interacts only weakly with the MoS_2 layers. Interestingly, while Ag has the lowest work function among the three metals, the overall interaction (charge transfer and interface stabilization) is intermediate between Cu and Au, indicating that interactions at the MoS_2 support interface are more complex beyond a simple charge-transfer picture as initially hypothesized. For the remainder of the paper, we focus on the interaction of adsorbates with Cu-supported MoS_2 phases wherein we expect to find maximum modulation of electronic properties of the MoS_2 layer by the TM support. Due to the computational cost of these models we restrict our attention to Cu(111) supports; results for the Cu(100) supports as expected to be qualitatively similar based on similar trends in the charge-transfer interactions [Fig. 3(c) and Fig. 3(d)].

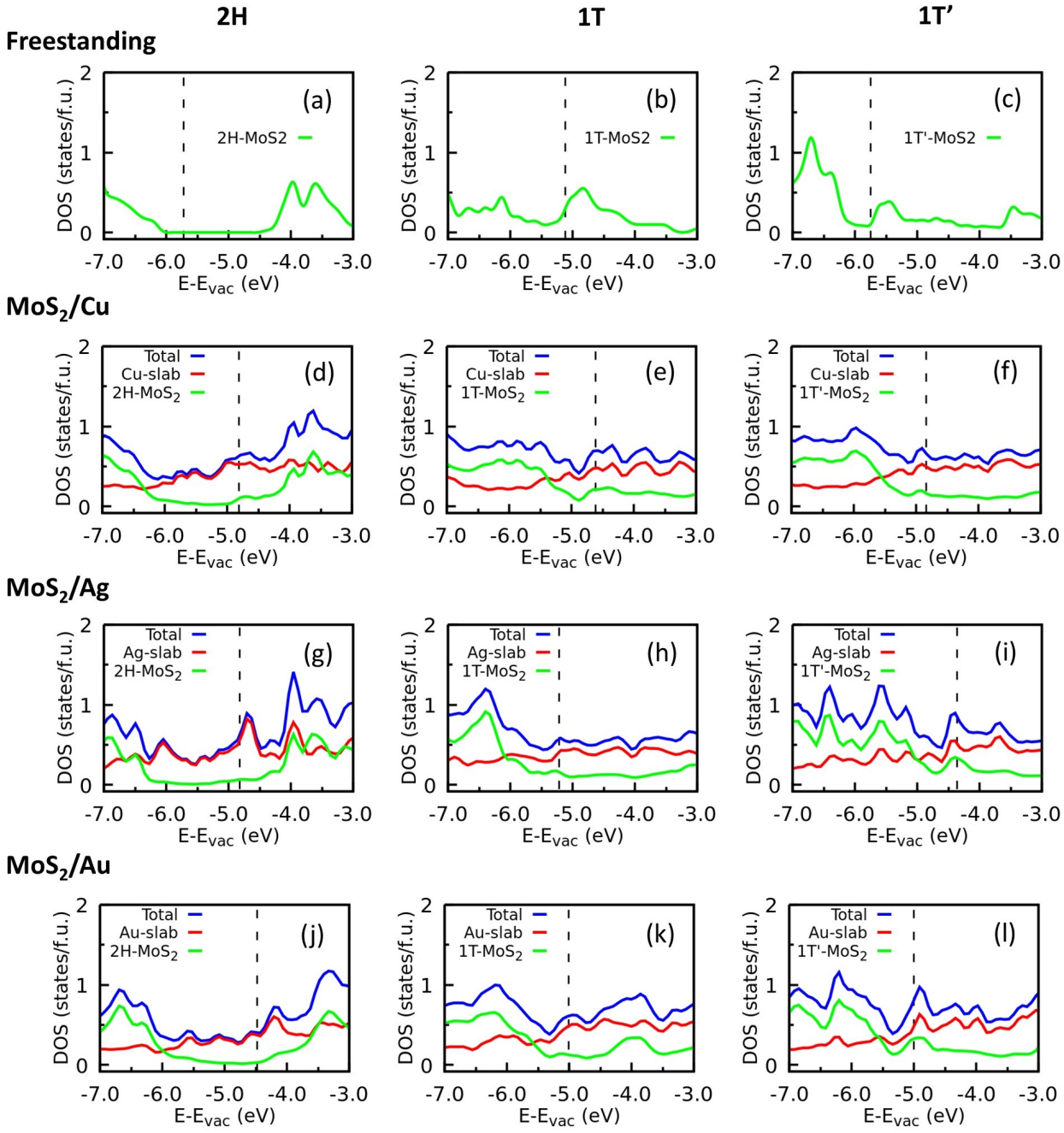

Figure 4: Density of states (DOS) per formula unit of MoS_2 for freestanding and TM supported monolayer-MoS_2. Total DOS (blue curve) for TM-supported slabs are decomposed into TM (red curve) and MoS_2 (green curve) contributions. Each column corresponds to a single phase while each row corresponds to a particular support (or lack thereof). The dashed line in each plot represents the Fermi level; the vacuum level, E_{vac}, is chosen as the zero of the energy scale.

3.2 Support Effects in CO- and H-Adsorption on MoS_2 Basal Planes

As noted previously, MoS_2 and similar TMDCs are being studied extensively for electrocatalytic CO2RR[10–12,16] and HER.[1,6,28] While the pathways for CO2RR can be quite complex—especially for the formation of higher hydrocarbons—in the case of C_1 products, CO is a key reaction intermediate for CO2RR.[65] In particular, CO gas can be a major product of CO2RR if CO desorbs easily from the catalyst surface; on the other hand, if CO is strongly bound by the catalyst, then it can be further reduced to form hydrocarbons.[16,57] In aqueous conditions, HER competes with CO2RR—usually for the same active site—and thus it is also necessary to understand this side reaction in relation to CO2RR. Here, we focus on understanding and comparing the adsorption of CO and H on various MoS_2 phases, considering both pristine basal planes and defective basal planes containing S vacancies. For now, we seek to understand the influence of support effects on molecular adsorption, using Cu(111) as a model support; we defer the study of MoS_2 edge sites to future work as there is the potential for complex bifunctional effects involving both MoS_2 as well as the support atoms, especially for supports such as Ag and Cu that are known to be active for CO2RR.[66–71]

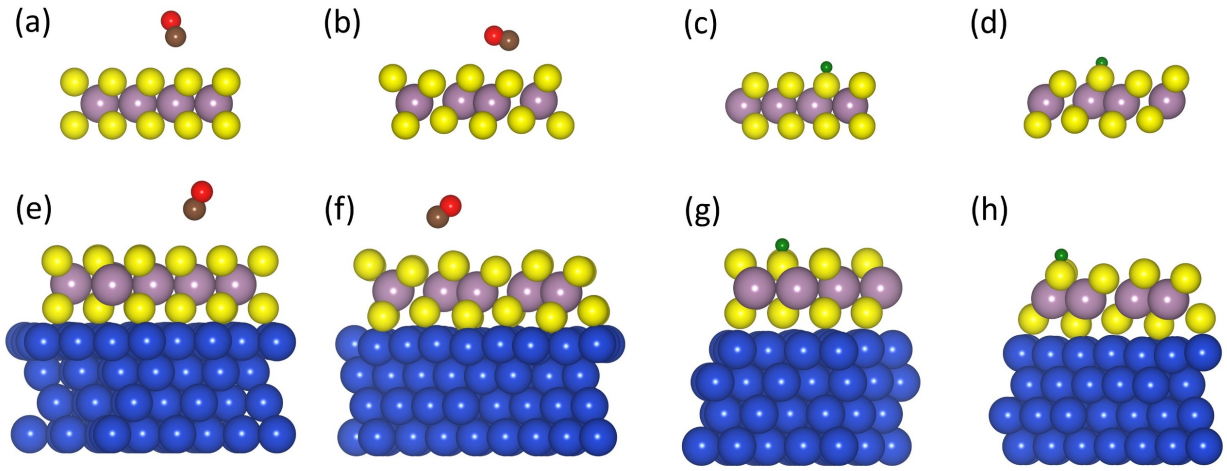

Figure 5: Freestanding MoS_2 monolayers with adsorbates: (a) CO on 2H MoS_2, (b) CO on 1T′ MoS_2, (c) H on 2H MoS_2, and (d) H on 1T′ MoS_2; Cu-supported MoS_2 monolayers with adsorbates: (e) CO on 2H MoS_2/Cu, (f) CO on 1T′ MoS_2/Cu, (g) H on 2H MoS_2/Cu, and (h) H on 1T′ MoS_2/Cu; Brown, red, yellow, cyan, blue, and green spheres represent C, O, S, Mo, Cu, and H atoms, respectively.

3.2.1 Adsorption on Basal Planes of Unsupported and Cu-Supported MoS_2

It is well known that the (pristine) basal plane of semiconducting 2H-MoS_2 is relatively inert towards adsorbates; metallic phases are much more active and are known to be good electrocatalysts for HER, in particular.[72,73] In Figure 5, we display the optimized atomic structures for H and CO adsorbed on freestanding and Cu-supported 2H and 1T′ MoS_2. In our DFT calculations of both CO and H adsorption, we find that the 1T phase, being the most thermodynamically unfavorable phase, undergoes a spontaneous adsorbate-induced phase transition to the lower energy 1T′ phase. Similar results have been noted in a previous DFT study.[74] Thus, adsorption on the 1T phase cannot be reported. The Gibbs free-energy of CO or H adsorption, ΔG_{ads} (ads = CO or H) is calculated as

$$\Delta G_{ads} = [E_{slab+ads} - E_{slab} - E_{ads} + \Delta E_{ZPE} + T\Delta S], \quad (3)$$

where $E_{slab+ads}$ is the DFT energy of the composite system composed of CO or H adsorbed on freestanding or Cu-supported MoS_2; $\underline{E}_{slab}$ is the energy of freestanding or Cu-supported MoS_2; E_{ads} is the energy of a CO molecule or half the energy of an H_2 molecule, both in their reference gas phases; and ΔE_{ZPE} and ΔS are the differences of zero-point energies and entropies of CO or H between their adsorbed and reference states. ΔE_{ZPE} + TΔS (at T=300K) is calculated as 0.25 eV, for H adsorption at the basal plane of 2H- and 1T'-MoS_2, while ΔE_{ZPE} + TΔS (at T=300K) for CO adsorption on the basal plane of 2H- and 1T'-MoS_2 are found to be 0.65 eV and 0.69 eV, respectively. We take these values of ΔE_{ZPE} + TΔS as representative for TM-supported MoS_2. The calculated adsorption free energies are displayed in Figure 6(a).

While the interaction of CO with 2H-MoS_2 is expected to be weak—CO is a closed shell molecule and the frontier orbitals of 2H-MoS_2 are also completely filled—interestingly, we find that the interaction with the metallic 1T′ phase is just as weak. On unsupported 2H- and 1T′-MoS_2, the CO molecule is physisorbed at nearly 3.5 Å from the sulfur plane (Fig. 5) with ΔG_{CO} of approximately 0.5 eV. This physisorbed state of CO is also observed on Cu-supported 2H- and 1T′-MoS_2 (Fig. 5) indicating that the charge transfer from Cu to MoS_2 has little to no effect on this adsorption process. The case of H adsorption is, however, quite different. On both unsupported and Cu-supported phases of 2H-MoS_2, H is chemisorbed but the thermodynamics is extremely unfavorable with ΔG_H = 1.88 eV on the unsupported monolayer and ΔG_H = 1.71 eV on the Cu-supported layer (Fig. 6). The slight decrease in ΔG_H by ~0.1 eV on the Cu-supported 2H phase is due to emergence of electronic states near the Fermi level as observed in Figure 4(d) and is comparable to our previous report for 2H-MoS_2 on Au supports,[37] with only a marginal improvement in thermodynamics due to the higher degree of charge transfer from Cu as compared to Au. On the 1T′ phase, however, the thermodynamics for H adsorption become quite favorable with a ΔG_H of 0.04 eV for an unsupported monolayer and 0.17 eV for the Cu-supported monolayer; note that these free energies approach the ideal value of $\Delta G_H \approx 0$ (Sabatier principle [54]) for

HER in the low overpotential range. It is interesting that the support now has a *detrimental* effect on the catalytic activity of the 1T′ phase as it reduces the propensity for H adsorption relative to the unsupported phase. This is an important observation as theoretical studies of 2D catalysts (especially high-throughput studies) tend to focus on unsupported layers for rational catalyst design whereas, in practice, support effects, as seen here, could introduce significant uncertainties in these predictions.

In summary, the basal plane of pristine 2H-MoS_2—supported or otherwise—is unsuited for CO2RR and HER. The basal plane of 1T′ MoS_2, on the other hand is already well suited for HER without any

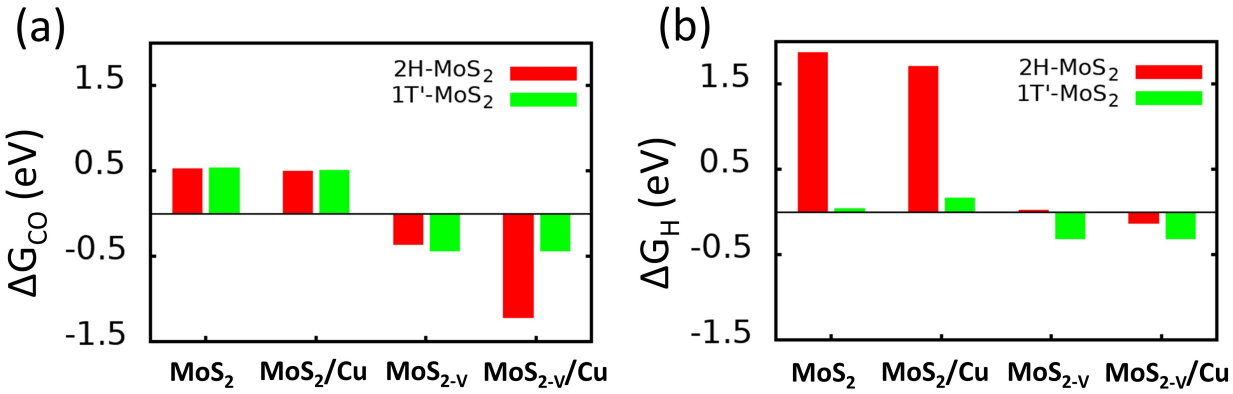

Figure 6: Free-energies of (a) CO adsorption (ΔG_{CO}) and (b) H adsorption (ΔG_H) on 2H and 1T′ phases of pristine MoS_2 monolayers and monolayers with a S vacancy($MoS_{2\text{-}V}$). When multiple stable adsorption sites exist, only the lowest adsorption free-energy (most stable adsorption configuration) is reported here.

further electron doping from the Cu support, which only has a detrimental effect; CO2RR is not viable though with or without electron doping from the Cu support.

3.2.2 Adsorption at Basal-Plane Sulfur Vacancies in Unsupported and Cu-Supported MoS_2

Although basal planes of MoS_2 are relatively chemically inert, S vacancies are well known to be catalytically active.[55,75,76] In addition to preexisting S vacancies, electrochemical desulfurization can also occur in working MoS_2 electrodes, further activating the basal planes of TMDs, for example, towards HER.[55,75] A recent computational study has also shown that basal plane vacancies in Group X TMDs are highly active and selective towards CO2RR.[77] Here, we seek to understand how interactions between 2H and 1T′ MoS_2 monolayers with Cu supports affects the catalytic behavior of basal-plane S vacancies.

Figure 7 displays optimized configurations of CO and H adsorbed at S vacancies in unsupported and Cu-supported 2H and 1T′ MoS_2 monolayers. As seen from the adsorption free-energies in Figure 6, both CO and H adsorption are thermodynamically favorable at S vacancies. Focusing on CO adsorption, there

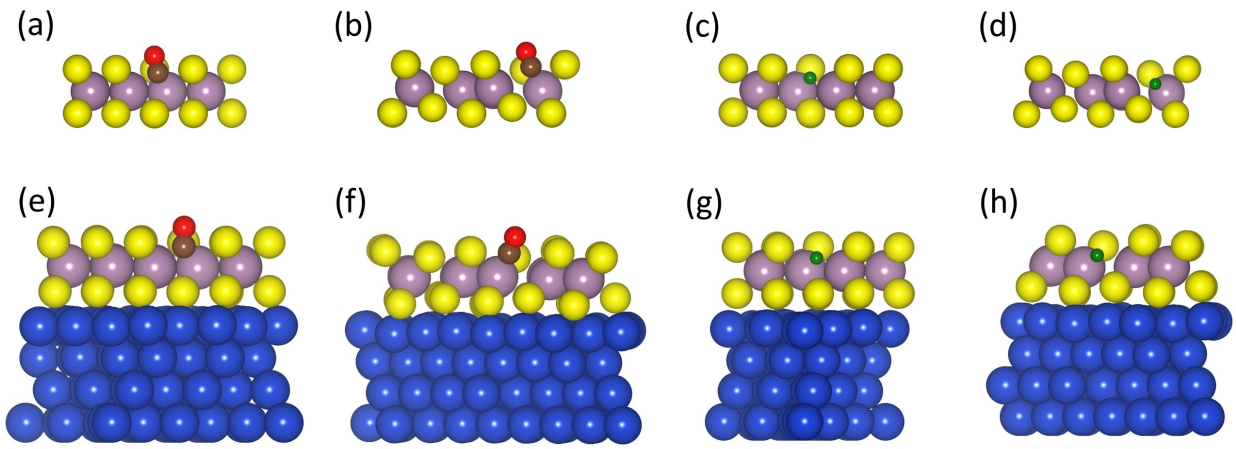

Figure 7: Freestanding MoS_2 containing a S-vacancy with adsorbates: (a) CO on 2H MoS_2; (b) CO on 1T′ MoS_2; (c) H on 2H MoS_2; (d) H on 1T′ MoS_2 is shown; Cu-supported MoS_2 slabs containing a S-vacancy with adsorbates: (e) CO on 2H MoS_2/Cu; (f) CO on 1T′ MoS_2/Cu; (g) H on 2H MoS_2/Cu; (h) H on 1T′ MoS_2/Cu is shown. Brown, red, yellow, cyan, blue, and green spheres represent C, O, S, Mo, Cu, and H atoms, respectively.

is little to no difference in ΔG_{CO} at the S vacancy in unsupported 2H and 1T′ monolayers. In the presence of the Cu support, ΔG_{CO} is relatively unaltered for the 1T′ phase but there is a significant increase in binding strength (ΔG_{CO} = -1.21 eV) for the 2H phase such that the S vacancy site will most likely be poisoned. This significant enhancement in CO binding occurs due to the emergence of new electronic states in MoS_2 near the Fermi level, arising from the interaction with the Cu support [Fig. S2(b)]. For completeness, we also tested CO adsorption at the S vacancy on Ag and Au supported monolayers and found ΔG_{CO} values of -1.02 eV and -1.05 eV, respectively. While a more comprehensive study of multiple supports, 2D materials, and adsorbates is deferred to future work, the current results already indicate that metal supports (or electrodes) are likely to play a significant role in the performance of TMDC electrocatalysts. In the case of H adsorption, the S vacancy site in the 2H phase is marginally unstable for HER and becomes thermodynamically stable (slightly negative ΔG_H) via interactions with the Cu support. In the case of the 1T′ phase, H adsorption is already favored ($\Delta G_H \sim$ -0.5 eV) in the unsupported case and is not altered any further by the Cu support. This is explained by the density of states [Fig. S2(c) and Fig.S2(d)], which shows no significant change near the Fermi level with or without the Cu support; in other words, 1T′ phase, being metallic, most likely screens out any charge-transfer dipoles at the 1T′-MoS_2/Cu interface.

In summary, we conclude that S vacancies in the 1T′ basal plane are relatively unaffected by the Cu support, and tend to overbind both CO and H. S vacancies in unsupported 2H-MoS_2 overbind CO but are almost ideal for HER. The Cu support effect is highly detrimental in the case of CO as it effectively leads to catalyst poisoning of basal plane S vacancies; the effect is less severe for H adsorption although far from ideal. Thus, it would appear from our calculations that S vacancies in unsupported 2H-MoS_2– possibly realized as nanoflowers or similar architectures—could offer a good compromise for both CO and H adsorption.

4. Conclusions

In conclusion, we employed DFT calculations to understand the interactions of monolayers of 2H, 1T, and 1T' phases with transition-metal supports, using Au, Ag, and Cu as model supports. Our calculations show that all phases of MoS_2 can form stable interfaces with the chosen TM supports and, in all cases, the Bader charge analysis show that the TM supports donate electrons to the MoS_2 monolayers with the extent of charge transfer being consistently higher for metallic 1T and 1T' phases of MoS_2 than for the semiconducting 2H phase. However, the extent of charge transfer is insufficient to induce a semiconductor-to-metal transition in the supported MoS_2 monolayers and the 2H-phase, which is the ground-state of the isolated monolayer, still remains the most stable phase on every TM support. Nevertheless, considering the higher density of electronic states appearing at the Fermi level of the 2H monolayer with increasing levels of charge transfer, we expect that the studied supports should, minimally, improve the electronic conductivity of semiconducting 2H-MoS_2.[37]

We also examined the role of the support in modulating the interaction of the supported monolayers with adsorbates such as H and CO whose adsorption free-energies can be considered as descriptors for HER and CO2RR. In the absence of any sulfur vacancy defects, the interaction of the MoS_2 basal plane with H and CO is weak (physisorption) irrespective of the support or the phase of MoS_2 that is employed. With the introduction of S vacancies, though, the studied adsorbates form strong chemical bonds at the undercoordinated vacancy site. While the free-energy for H adsorption is only slightly perturbed by the presence of the Cu support, the effect on CO adsorption is rather significant to the extent that the S vacancy sites in 2H MoS_2 are likely to be poisoned by CO when supported on Cu. The support effect is almost negligible on the 1T' phase although both H and CO are slightly overbound. In short, our studies unambiguously demonstrate that support effects cannot be neglected when trying to establish the relative merits of various 2D TMD catalysts, especially in the presence of charge transfer interactions as might be expected at interfaces between electrodes and the TMD catalyst.

Supporting Information

Comparison of models with different mismatch strains between supported MoS_2 monolayers and TM slabs; Density of states for 2H and 1T′ MoS_2 containing a sulfur vacancy with and without Cu(111) supports; Optimized MoS_2/TM supercells in VASP format

Acknowledgements

We gratefully acknowledge research support from the National Science Foundation (NSF-CBET-1803614) and the United States–Israel Binational Science Foundation (NSF-BSF CBET 2017642). This work used the Extreme Science and Engineering Discovery Environment (XSEDE), which is supported by National Science Foundation grant number ACI-1548562.

References

(1) Yang, L.; Liu, P.; Li, J.; Xiang, B. Two-Dimensional Material Molybdenum Disulfides as Electrocatalysts for Hydrogen Evolution. *Catalysts* **2017**, *7* (10) DOI: 10.3390/catal7100285.

(2) Theerthagiri, J.; Senthil, R. A.; Senthilkumar, B.; Reddy Polu, A.; Madhavan, J.; Ashokkumar, M. Recent Advances in MoS2 Nanostructured Materials for Energy and Environmental Applications – A Review. *J. Solid State Chem.* **2017**, *252*, 43–71 DOI: https://doi.org/10.1016/j.jssc.2017.04.041.

(3) Li, F. Two-Dimensional Transition Metal Dichalcogenides for Electrocatalytic Energy Conversion Applications; Nayak, M. X. E.-P. K., Ed.; IntechOpen: Rijeka, 2016; p Ch. 4.

(4) Chia, X.; Eng, A. Y. S.; Ambrosi, A.; Tan, S. M.; Pumera, M. Electrochemistry of Nanostructured Layered Transition-Metal Dichalcogenides. *Chem. Rev.* **2015**, *115* (21), 11941–11966 DOI: 10.1021/acs.chemrev.5b00287.

(5) Chia, X.; Pumera, M. Characteristics and Performance of Two-Dimensional Materials for Electrocatalysis. *Nat. Catal.* **2018**, *1* (12), 909–921 DOI: 10.1038/s41929-018-0181-7.

(6) Zhang, G.; Liu, H.; Qu, J.; Li, J. Two-Dimensional Layered MoS2: Rational Design{,} Properties and Electrochemical Applications. *Energy Environ. Sci.* **2016**, *9* (4), 1190–1209 DOI: 10.1039/C5EE03761A.

(7) Chianelli, R. R.; Siadati, M. H.; De la Rosa, M. P.; Berhault, G.; Wilcoxon, J. P.; Bearden, R.; Abrams, B. L. Catalytic Properties of Single Layers of Transition Metal Sulfide Catalytic Materials. *Catal. Rev.* **2006**, *48* (1), 1–41 DOI: 10.1080/01614940500439776.

(8) Jaramillo, T. F.; Jørgensen, K. P.; Bonde, J.; Nielsen, J. H.; Horch, S.; Chorkendorff, I.

Identification of Active Edge Sites for Electrochemical H2 Evolution from MoS2 Nanocatalysts. *Science (80-.).* **2007**, *317* (5834), 100–102 DOI: 10.1126/science.1141483.

(9) Wang, T.; Gao, D.; Zhuo, J.; Zhu, Z.; Papakonstantinou, P.; Li, Y.; Li, M. Size-Dependent Enhancement of Electrocatalytic Oxygen-Reduction and Hydrogen-Evolution Performance of MoS2 Particles. *Chem. – A Eur. J.* **2013**, *19* (36), 11939–11948 DOI: 10.1002/chem.201301406.

(10) Asadi, M.; Kumar, B.; Behranginia, A.; Rosen, B. A.; Baskin, A.; Repnin, N.; Pisasale, D.; Phillips, P.; Zhu, W.; Haasch, R.; *et al*. Robust Carbon Dioxide Reduction on Molybdenum Disulphide Edges. *Nat. Commun.* **2014**, *5* (1), 4470 DOI: 10.1038/ncomms5470.

(11) Asadi, M.; Kim, K.; Liu, C.; Addepalli, A. V.; Abbasi, P.; Yasaei, P.; Phillips, P.; Behranginia, A.; Cerrato, J. M.; Haasch, R.; *et al.* Nanostructured Transition Metal Dichalcogenide Electrocatalysts for CO_2 Reduction in Ionic Liquid. *Science (80-.).* **2016**, *353* (6298), 467–470 DOI: 10.1126/science.aaf4767.

(12) Abbasi, P.; Asadi, M.; Liu, C.; Sharifi-Asl, S.; Sayahpour, B.; Behranginia, A.; Zapol, P.; Shahbazian-Yassar, R.; Curtiss, L. A.; Salehi-Khojin, A. Tailoring the Edge Structure of Molybdenum Disulfide toward Electrocatalytic Reduction of Carbon Dioxide. *ACS Nano* **2017**, *11* (1), 453–460 DOI: 10.1021/acsnano.6b06392.

(13) Rani, B. J.; Pradeepa, S. S.; Hasan, Z. M.; Ravi, G.; Yuvakkumar, R.; Hong, S. I. Supercapacitor and OER Activity of Transition Metal (Mo, Co, Cu) Sulphides. *J. Phys. Chem. Solids* **2020**, *138*, 109240 DOI: https://doi.org/10.1016/j.jpcs.2019.109240.

(14) Ding, X.; Li, X.; Lv, X.; Zheng, Y.-Z.; Wu, Q.; Ding, H.; Wu, J.; Li, R.; Tao, X. Composition Engineering–Triggered Bifunctionality of Free-Standing Coral-Like 1T-MoS_2 for Highly Efficient Overall Water Splitting. *Energy Technol. n/a* (n/a), 2000268 DOI: 10.1002/ente.202000268.

(15) Liu, Y.; Jiang, S.; Li, S.; Zhou, L.; Li, Z.; Li, J.; Shao, M. Interface Engineering of (Ni, Fe)S_2@MoS_2 Heterostructures for Synergetic Electrochemical Water Splitting. *Appl. Catal. B Environ.* **2019**, *247*, 107–114 DOI: https://doi.org/10.1016/j.apcatb.2019.01.094.

(16) Chan, K.; Tsai, C.; Hansen, H. A.; Nørskov, J. K. Molybdenum Sulfides and Selenides as Possible Electrocatalysts for CO_2 Reduction. *ChemCatChem* **2014**, *6* (7), 1899–1905 DOI: 10.1002/cctc.201402128.

(17) Francis, S. A.; Velazquez, J. M.; Ferrer, I. M.; Torelli, D. A.; Guevarra, D.; McDowell, M. T.; Sun, K.; Zhou, X.; Saadi, F. H.; John, J.; *et al.* Reduction of Aqueous CO_2 to 1-Propanol at MoS_2 Electrodes. *Chem. Mater.* **2018**, *30* (15), 4902–4908 DOI: 10.1021/acs.chemmater.7b04428.

(18) Lau, T. H. .; Wu, S.; Kato, R.; Wu, T.-S.; Kulhavy, J.; Mo, J.; Zheng, J.; Foord, J. S.; Soo, Y.-L.;

Suenaga, K.; *et al*. Engineering Monolayer 1T-MoS_2 into a Bifunctional Electrocatalyst via Sonochemical Doping of Isolated Transition Metal Atoms. *ACS Catal.* **2019**, acscatal.9b01503 DOI: 10.1021/acscatal.9b01503.

(19) Li, G.; Chen, Z.; Li, Y.; Zhang, D.; Yang, W.; Liu, Y.; Cao, L. Engineering Substrate Interaction To Improve Hydrogen Evolution Catalysis of Monolayer MoS_2 Films beyond Pt. *ACS Nano* **2020**, *14* (2), 1707–1714 DOI: 10.1021/acsnano.9b07324.

(20) Luo, R.; Luo, M.; Wang, Z.; Liu, P.; Song, S.; Wang, X.; Chen, M. The Atomic Origin of Nickel-Doping-Induced Catalytic Enhancement in MoS_2 for Electrochemical Hydrogen Production. *Nanoscale* **2019**, *11* (15), 7123–7128 DOI: 10.1039/C8NR10023C.

(21) Zhang, X.; Zhou, F.; Zhang, S.; Liang, Y.; Wang, R. Engineering MoS_2 Basal Planes for Hydrogen Evolution via Synergistic Ruthenium Doping and Nanocarbon Hybridization. *Adv. Sci.* **2019**, *6* (10), 1900090 DOI: 10.1002/advs.201900090.

(22) Gao, C.; Hua, H.; Du, M.; Liu, J.; Wu, X.; Pu, Y.; Li, X. 1T/2H MoS_2 Nanoflowers Decorated Amorphous Mo-CoS_x Skeleton: A ZIF-Based Composite Electrocatalyst for the Hydrogen Evolution Reaction. *Appl. Surf. Sci.* **2020**, *515*, 145842 DOI: https://doi.org/10.1016/j.apsusc.2020.145842.

(23) Zhang, J.; Xu, X.; Yang, L.; Cheng, D.; Cao, D. Single-Atom Ru Doping Induced Phase Transition of MoS_2 and S Vacancy for Hydrogen Evolution Reaction. *Small Methods* **2019**, *3* (12), 1900653 DOI: 10.1002/smtd.201900653.

(24) Kibsgaard, J.; Chen, Z.; Reinecke, B. N.; Jaramillo, T. F. Engineering the Surface Structure of MoS_2 to Preferentially Expose Active Edge Sites for Electrocatalysis. *Nat. Mater.* **2012**, *11* (11), 963–969 DOI: 10.1038/nmat3439.

(25) Hu, J.; Huang, B.; Zhang, C.; Wang, Z.; An, Y.; Zhou, D.; Lin, H.; Leung, M. K. H.; Yang, S. Engineering Stepped Edge Surface Structures of MoS_2 Sheet Stacks to Accelerate the Hydrogen Evolution Reaction. *Energy Environ. Sci.* **2017**, *10* (2), 593–603 DOI: 10.1039/C6EE03629E.

(26) Wang, H.; Zhang, Q.; Yao, H.; Liang, Z.; Lee, H.-W.; Hsu, P.-C.; Zheng, G.; Cui, Y. High Electrochemical Selectivity of Edge versus Terrace Sites in Two-Dimensional Layered MoS_2 Materials. *Nano Lett.* **2014**, *14* (12), 7138–7144 DOI: 10.1021/nl503730c.

(27) Yin, Y.; Han, J.; Zhang, Y.; Zhang, X.; Xu, P.; Yuan, Q.; Samad, L.; Wang, X.; Wang, Y.; Zhang, Z.; *et al*. Contributions of Phase, Sulfur Vacancies, and Edges to the Hydrogen Evolution Reaction Catalytic Activity of Porous Molybdenum Disulfide Nanosheets. *J. Am. Chem. Soc.* **2016**, *138* (25), 7965–7972 DOI: 10.1021/jacs.6b03714.

(28) Voiry, D.; Salehi, M.; Silva, R.; Fujita, T.; Chen, M.; Asefa, T.; Shenoy, V. B.; Eda, G.;

Chhowalla, M. Conducting MoS_2 Nanosheets as Catalysts for Hydrogen Evolution Reaction. *Nano Lett.* **2013**, *13* (12), 6222–6227 DOI: 10.1021/nl403661s.

(29) Lukowski, M. A.; Daniel, A. S.; Meng, F.; Forticaux, A.; Li, L.; Jin, S. Enhanced Hydrogen Evolution Catalysis from Chemically Exfoliated Metallic MoS_2 Nanosheets. *J. Am. Chem. Soc.* **2013**, *135* (28), 10274–10277 DOI: 10.1021/ja404523s.

(30) Bissessur, R.; Kanatzidis, M. G.; Schindler, J. L.; Kannewurf, C. R. Encapsulation of Polymers into MoS_2 and Metal to Insulator Transition in Metastable MoS_2. *J. Chem. Soc. Chem. Commun.* **1993**, No. 20, 1582–1585 DOI: 10.1039/C39930001582.

(31) Kan, M.; Wang, J. Y.; Li, X. W.; Zhang, S. H.; Li, Y. W.; Kawazoe, Y.; Sun, Q.; Jena, P. Structures and Phase Transition of a MoS_2 Monolayer. *J. Phys. Chem. C* **2014**, *118* (3), 1515–1522 DOI: 10.1021/jp4076355.

(32) Huang, H. H.; Fan, X.; Singh, D. J.; Zheng, W. T. First Principles Study on 2H–1T′ Transition in MoS_2 with Copper. *Phys. Chem. Chem. Phys.* **2018**, *20* (42), 26986–26994 DOI: 10.1039/C8CP05445B.

(33) Gan, X.; Lee, L. Y. S.; Wong, K.; Lo, T. W.; Ho, K. H.; Lei, D. Y.; Zhao, H. 2H/1T Phase Transition of Multilayer MoS_2 by Electrochemical Incorporation of S Vacancies. *ACS Appl. Energy Mater.* **2018**, *1* (9), 4754–4765 DOI: 10.1021/acsaem.8b00875.

(34) Jin, Q.; Liu, N.; Chen, B.; Mei, D. Mechanisms of Semiconducting 2H to Metallic 1T Phase Transition in Two-Dimensional MoS_2 Nanosheets. *J. Phys. Chem. C* **2018**, *122* (49), 28215–28224 DOI: 10.1021/acs.jpcc.8b10256.

(35) Lin, Y.-C.; Dumcenco, D. O.; Huang, Y.-S.; Suenaga, K. Atomic Mechanism of the Semiconducting-to-Metallic Phase Transition in Single-Layered MoS_2. *Nat. Nanotechnol.* **2014**, *9* (5), 391–396 DOI: 10.1038/nnano.2014.64.

(36) Kappera, R.; Voiry, D.; Yalcin, S. E.; Branch, B.; Gupta, G.; Mohite, A. D.; Chhowalla, M. Phase-Engineered Low-Resistance Contacts for Ultrathin MoS_2 Transistors. *Nat. Mater.* **2014**, *13* (12), 1128–1134 DOI: 10.1038/nmat4080.

(37) Bar-Ziv, R.; Ranjan, P.; Lavie, A.; Jain, A.; Garai, S.; Bar Hen, A.; Popovitz-Biro, R.; Tenne, R.; Arenal, R.; Ramasubramaniam, A.; *et al*. Au-MoS_2 Hybrids as Hydrogen Evolution Electrocatalysts. *ACS Appl. Energy Mater.* **2019**, *2* (8), 6043–6050 DOI: 10.1021/acsaem.9b01147.

(38) Maiti, P. S.; Ganai, A. K.; Bar-Ziv, R.; Enyashin, A. N.; Houben, L.; Bar Sadan, M. Cu_2–XS–MoS_2 Nano-Octahedra at the Atomic Scale: Using a Template To Activate the Basal Plane of MoS2 for Hydrogen Production. *Chem. Mater.* **2018**, *30* (14), 4489–4492 DOI:

10.1021/acs.chemmater.8b01239.

(39) Chen, J.; Liu, G.; Zhu, Y.; Su, M.; Yin, P.; Wu, X.; Lu, Q.; Tan, C.; Zhao, M.; Liu, Z.; *et al*. Ag@MoS_2 Core–Shell Heterostructure as SERS Platform to Reveal the Hydrogen Evolution Active Sites of Single-Layer MoS2. *J. Am. Chem. Soc.* **2020**, *142* (15), 7161–7167 DOI: 10.1021/jacs.0c01649.

(40) Kresse, G.; Furthmüller, J. Efficient Iterative Schemes for Ab Initio Total-Energy Calculations Using a Plane-Wave Basis Set. *Phys. Rev. B* **1996**, *54* (16), 11169–11186 DOI: 10.1103/PhysRevB.54.11169.

(41) Kresse, G.; Furthmüller, J. Efficiency of Ab-Initio Total Energy Calculations for Metals and Semiconductors Using a Plane-Wave Basis Set. *Comput. Mater. Sci.* **1996**, *6* (1), 15–50 DOI: 10.1016/0927-0256(96)00008-0.

(42) Blöchl, P. E. Projector Augmented-Wave Method. *Phys. Rev. B* **1994**, *50* (24), 17953–17979 DOI: 10.1103/PhysRevB.50.17953.

(43) Kresse, G.; Joubert, D. From Ultrasoft Pseudopotentials to the Projector Augmented-Wave Method. *Phys. Rev. B* **1999**, *59* (3), 1758–1775 DOI: 10.1103/PhysRevB.59.1758.

(44) Perdew, J. P.; Burke, K.; Ernzerhof, M. Generalized Gradient Approximation Made Simple. *Phys. Rev. Lett.* **1996**, *77* (18), 3865–3868 DOI: 10.1103/PhysRevLett.77.3865.

(45) He, H.; Lu, P.; Wu, L.; Zhang, C.; Song, Y.; Guan, P.; Wang, S. Structural Properties and Phase Transition of Na Adsorption on Monolayer MoS_2. *Nanoscale Res. Lett.* **2016**, *11* (1), 330 DOI: 10.1186/s11671-016-1550-2.

(46) Qian, X.; Liu, J.; Fu, L.; Li, J. Quantum Spin Hall Effect in Two-Dimensional Transition Metal Dichalcogenides. *Science (80-.).* **2014**, *346* (6215), 1344–1347 DOI: 10.1126/science.1256815.

(47) Haas, P.; Tran, F.; Blaha, P. Calculation of the Lattice Constant of Solids with Semilocal Functionals. *Phys. Rev. B* **2009**, *79* (8), 85104 DOI: 10.1103/PhysRevB.79.085104.

(48) Lazić, P. CellMatch: Combining Two Unit Cells into a Common Supercell with Minimal Strain. *Comput. Phys. Commun.* **2015**, *197*, 324–334 DOI: 10.1016/J.CPC.2015.08.038.

(49) Makov, G.; Payne, M. C. Periodic Boundary Conditions in *Ab Initio* Calculations. *Phys. Rev. B* **1995**, *51* (7), 4014–4022 DOI: 10.1103/PhysRevB.51.4014.

(50) Neugebauer, J.; Scheffler, M. Adsorbate-Substrate and Adsorbate-Adsorbate Interactions of Na and K Adlayers on Al(111). *Phys. Rev. B* **1992**, *46* (24), 16067–16080 DOI: 10.1103/PhysRevB.46.16067.

(51) Henkelman, G.; Arnaldsson, A.; Jónsson, H. A Fast and Robust Algorithm for Bader Decomposition of Charge Density. *Comput. Mater. Sci.* **2006**, *36* (3), 354–360 DOI:

https://doi.org/10.1016/j.commatsci.2005.04.010.

(52) Sanville, E.; Kenny, S. D.; Smith, R.; Henkelman, G. Improved Grid-Based Algorithm for Bader Charge Allocation. *J. Comput. Chem.* **2007**, *28* (5), 899–908 DOI: 10.1002/jcc.20575.

(53) Tang, W.; Sanville, E.; Henkelman, G. A Grid-Based Bader Analysis Algorithm without Lattice Bias. *J. Phys. Condens. Matter* **2009**, *21* (8), 084204 DOI: 10.1088/0953-8984/21/8/084204.

(54) Grimme, S.; Antony, J.; Ehrlich, S.; Krieg, H. A Consistent and Accurate Ab Initio Parametrization of Density Functional Dispersion Correction (DFT-D) for the 94 Elements H-Pu. *J. Chem. Phys.* **2010**, *132* (15), 154104 DOI: 10.1063/1.3382344.

(55) Li, H.; Tsai, C.; Koh, A. L.; Cai, L.; Contryman, A. W.; Fragapane, A. H.; Zhao, J.; Han, H. S.; Manoharan, H. C.; Abild-Pedersen, F.; *et al*. Activating and Optimizing MoS_2 Basal Planes for Hydrogen Evolution through the Formation of Strained Sulphur Vacancies. *Nat. Mater.* **2016**, *15* (1), 48–53 DOI: 10.1038/nmat4465.

(56) Tsai, C.; Chan, K.; Nørskov, J. K.; Abild-Pedersen, F. Theoretical Insights into the Hydrogen Evolution Activity of Layered Transition Metal Dichalcogenides. *Surf. Sci.* **2015**, *640*, 133–140 DOI: 10.1016/j.susc.2015.01.019.

(57) Shin, H.; Ha, Y.; Kim, H. 2D Covalent Metals: A New Materials Domain of Electrochemical CO2 Conversion with Broken Scaling Relationship. *J. Phys. Chem. Lett.* **2016**, *7* (20), 4124–4129 DOI: 10.1021/acs.jpclett.6b01876.

(58) Reuter, K.; Stampf, C.; Scheffler, M. AB Initio Atomistic Thermodynamics and Statistical Mechanics of Surface Properties and Functions BT - Handbook of Materials Modeling: Methods; Yip, S., Ed.; Springer Netherlands: Dordrecht, 2005; pp 149–194.

(59) Johnson III, R. D. NIST 101. *Comput. Chem. Comp. Benchmark Database* **1999**.

(60) Enyashin, A. N.; Seifert, G. Electronic Properties of MoS_2 Monolayer and Related Structures. *Nanosyst. PHYSICS, Chem. Math.* **2014**, *5* (4), 517–539.

(61) Kang, Y.; Najmaei, S.; Liu, Z.; Bao, Y.; Wang, Y.; Zhu, X.; Halas, N. J.; Nordlander, P.; Ajayan, P. M.; Lou, J.; *et al*. Plasmonic Hot Electron Induced Structural Phase Transition in a MoS_2 Monolayer. *Adv. Mater.* **2014**, *26* (37), 6467–6471 DOI: 10.1002/adma.201401802.

(62) Yang, D.; Sandoval, S. J.; Divigalpitiya, W. M. R.; Irwin, J. C.; Frindt, R. F. Structure of Single-Molecular-Layer MoS_2. *Phys. Rev. B* **1991**, *43* (14), 12053–12056 DOI: 10.1103/PhysRevB.43.12053.

(63) Heising, J.; Kanatzidis, M. G. Structure of Restacked MoS_2 and WS_2 Elucidated by Electron Crystallography. *J. Am. Chem. Soc.* **1999**, *121* (4), 638–643 DOI: 10.1021/ja983043c.

(64) Sun, X.; Wang, Z.; Li, Z.; Fu, Y. Q. Origin of Structural Transformation in Mono- and Bi-

Layered Molybdenum Disulfide. *Sci. Rep.* **2016**, *6* (1), 26666 DOI: 10.1038/srep26666.

(65) Kortlever, R.; Shen, J.; Schouten, K. J. P.; Calle-Vallejo, F.; Koper, M. T. M. Catalysts and Reaction Pathways for the Electrochemical Reduction of Carbon Dioxide. *J. Phys. Chem. Lett.* **2015**, *6* (20), 4073–4082 DOI: 10.1021/acs.jpclett.5b01559.

(66) Ma, M.; Djanashvili, K.; Smith, W. A. Controllable Hydrocarbon Formation from the Electrochemical Reduction of CO_2 over Cu Nanowire Arrays. *Angew. Chemie Int. Ed.* **2016**, *55* (23), 6680–6684 DOI: 10.1002/anie.201601282.

(67) Ma, S.; Lan, Y.; Perez, G. M. J.; Moniri, S.; Kenis, P. J. A. Silver Supported on Titania as an Active Catalyst for Electrochemical Carbon Dioxide Reduction. *ChemSusChem* **2014**, *7* (3), 866–874 DOI: 10.1002/cssc.201300934.

(68) Hatsukade, T.; Kuhl, K. P.; Cave, E. R.; Abram, D. N.; Jaramillo, T. F. Insights into the Electrocatalytic Reduction of CO_2 on Metallic Silver Surfaces. *Phys. Chem. Chem. Phys.* **2014**, *16* (27), 13814–13819 DOI: 10.1039/C4CP00692E.

(69) Reske, R.; Mistry, H.; Behafarid, F.; Roldan Cuenya, B.; Strasser, P. Particle Size Effects in the Catalytic Electroreduction of CO_2 on Cu Nanoparticles. *J. Am. Chem. Soc.* **2014**, *136* (19), 6978–6986 DOI: 10.1021/ja500328k.

(70) Manthiram, K.; Beberwyck, B. J.; Alivisatos, A. P. Enhanced Electrochemical Methanation of Carbon Dioxide with a Dispersible Nanoscale Copper Catalyst. *J. Am. Chem. Soc.* **2014**, *136* (38), 13319–13325 DOI: 10.1021/ja5065284.

(71) Huang, J.; Mensi, M.; Oveisi, E.; Mantella, V.; Buonsanti, R. Structural Sensitivities in Bimetallic Catalysts for Electrochemical CO_2 Reduction Revealed by Ag–Cu Nanodimers. *J. Am. Chem. Soc.* **2019**, *141* (6), 2490–2499 DOI: 10.1021/jacs.8b12381.

(72) Liu, Z.; Zhang, X.; Gong, Y.; Lu, Q.; Zhang, Z.; Cheng, H.; Ma, Q.; Chen, J.; Zhao, M.; Chen, B.; *et al*. Synthesis of MoX_2 (X = Se or S) Monolayers with High-Concentration 1T′ Phase on 4H/Fcc-Au Nanorods for Hydrogen Evolution. *Nano Res.* **2019**, *12* (6), 1301–1305 DOI: 10.1007/s12274-018-2212-8.

(73) Sun, K.; Liu, Y.; Pan, Y.; Zhu, H.; Zhao, J.; Zeng, L.; Liu, Z.; Liu, C. Targeted Bottom-up Synthesis of 1T-Phase MoS_2 Arrays with High Electrocatalytic Hydrogen Evolution Activity by Simultaneous Structure and Morphology Engineering. *Nano Res.* **2018**, *11* (8), 4368–4379 DOI: 10.1007/s12274-018-2026-8.

(74) Tang, Q.; Jiang, D. Mechanism of Hydrogen Evolution Reaction on 1T-MoS_2 from First Principles. *ACS Catal.* **2016**, *6* (8), 4953–4961 DOI: 10.1021/acscatal.6b01211.

(75) Tsai, C.; Li, H.; Park, S.; Park, J.; Han, H. S.; Nørskov, J. K.; Zheng, X.; Abild-Pedersen, F.

Electrochemical Generation of Sulfur Vacancies in the Basal Plane of MoS_2 for Hydrogen Evolution. *Nat. Commun.* **2017**, *8* (1), 15113 DOI: 10.1038/ncomms15113.

(76) Le, D.; Rawal, T. B.; Rahman, T. S. Single-Layer MoS_2 with Sulfur Vacancies: Structure and Catalytic Application. *J. Phys. Chem. C* **2014**, *118* (10), 5346–5351 DOI: 10.1021/jp411256g.

(77) Ji, Y.; Nørskov, J. K.; Chan, K. Scaling Relations on Basal Plane Vacancies of Transition Metal Dichalcogenides for CO2 Reduction. *J. Phys. Chem. C* **2019**, *123* (7), 4256–4261 DOI: 10.1021/acs.jpcc.8b11628.

TOC GRAPHIC